INTERNATIONAL JOURNAL FOR NUMERICAL AND ANALYTICAL METHODS IN GEOMECHANICS
*Int. J. Numer. Anal. Meth. Geomech.* 2008; **32**:509–522
Published online 12 June 2007 in Wiley InterScience (www.interscience.wiley.com). DOI: 10.1002/nag.635

# A note on the generation of periodic granular microstructures based on grain size distributions

H. A. Meier[1], E. Kuhl[2,*,†] and P. Steinmann[2]

[1]*Chair of Applied Mechanics, Department of Mechanical Engineering, University of Kaiserslautern, Germany*
[2]*Department of Mechanical Engineering, Stanford University, Stanford, CA 94305-4040, U.S.A.*

SUMMARY

This short communication discusses an algorithm suited for the generation of periodic microstructures of granular media. Its particular features are a user-defined grain size distribution, a representative volume element which is intrinsically periodic *ab initio* and a user-defined termination criterion, controlled by an increase of volume fraction. For low densities our particle packings resemble fluids or gases, while we aim to reach for rather dense particle packings, similar to granular solids. The generated microstructures can thus be readily incorporated into large multiscale simulations, e.g. on the integration point level of a finite element analysis of a particular sand or concrete. The individual grain size distribution of the granular medium is incorporated through the introduction of different growth rates governing the final particle size distribution. We briefly sketch the generation of the representative volume element within a serial event-driven scheme and demonstrate how periodic boundary conditions are ensured throughout the representative volume element generation process. The potential of the suggested algorithm will be illustrated through the generation of two different periodic multi-disperse microstructures. They are based on different given grain size distributions, one for a quartz sand with a low non-uniformity index and one for concrete aggregates classified as A32 by the German standard norm DIN 1045 to have a rather large variation in grain size. Copyright © 2007 John Wiley & Sons, Ltd.

Received 30 November 2006; Revised 23 April 2007; Accepted 29 April 2007

KEY WORDS: representative volume element; periodic microstructure; grain size distribution; quartz; concrete

## 1. INTRODUCTION

Analysis of granular media can be accomplished in many ways. Next to the approach of assuming a continuum, a dis-continuum can be set up. A dis-continuum which consists of a finite number

*Correspondence to: E. Kuhl, Department of Mechanical Engineering, Stanford University, Stanford, CA 94305-4040, U.S.A.
†E-mail: ekuhl@stanford.edu

Contract/grant sponsor: DFG International Research Training Group 1131

of discrete particles is capable of capturing the behaviour of granular media in a natural way. In contrast to continuum-based simulations, discrete particle simulations allow single grains to form clusters and break contacts. This behaviour is distinguishing for particulate media and is directly related to the failure characteristics of granular assemblies. The most prominent algorithm that traces the behaviour of granular assemblies is with no doubt the discrete element method (dem) by Cundall and Strack [1, 2].

The major drawback of the dem is obviously the fact that it is extremely costly from a computational point of view such that analyses are usually limited to small specimen. Nevertheless, when combined with appropriate homogenization techniques, particle methods can be used as a powerful and effective tool to model large-scale structures consisting of granular media, see e.g. Zohdi [3–5]. Such homogenization techniques typically focus on the analysis of small periodic representative units, see e.g. Luding [6, 7]. Assuming that the number of particles (nop) inside these periodic volume elements are capable of reproducing the behaviour of the whole granular medium, the periodic volume elements can be considered to be representative, see e.g. Stroeven *et al.* [8] or Gitman *et al.* [9]. The representative volume element (rve) enables to restrict the computational effort to the smallest, still representative, material sample.

Although theoretically well understood, the efficient construction of an rve having a high-volume fraction and at the same time being irregular regarding the particle set-up is part of intensive research. We would like to draw the attention of the geo-mechanical community to a class of particle packing methods developed in computational chemistry. These packing methods are extremely efficient and their outcome is congruent with the expectations of an irregular highly packed geometrically periodic representative volume element used in geo-mechanical multiscale methods, see Lubachevsky *et al.* [10–12] for the original algorithm and Meier *et al.* [13, 14] for additional information. In contrast to the vast majority of rve generation schemes, the Lubachevsky–Stillinger algorithm is capable to incorporate geometric periodic boundaries in a natural way. Opposed to Burner *et al.* [15], Lätzel *et al.* [16], Luding [6] and Luding and Santos [17], who analyse granular assemblies as such on the microscopic scale, we aim at generating microstructures which are periodic *ab initio* with the ultimate goal of embedding those in a macroscopic finite element analysis. This manuscript illustrates our first steps along these lines. In the following, we will demonstrate how prescribed given grain size distributions can be incorporated straightforwardly in the classical Lubachevsky–Stillinger approach. Note, we do not aim to reach the highest possible packing density, rather than to produce a packing of particles, possessing geometric periodic boundaries, which is suitable in a multiscale approach, see [13, 18]. For high packing densities we refer the interested reader to [19] and references therein. In summary, the algorithm presented here is used as a preprocessor, generating geometrically periodic rves, which are based on a given grain size distribution. Embedding, as well as further computation of the results here, is not the focal point presented of this manuscript.

The manuscript is organized as follows. In Section 2, we illustrate the overall algorithmic set-up to generate periodic granular microstructures within an event-driven scheme. In particular, we illustrate how the time step size can be calculated and how the event itself is handled. Next, in Section 3, the concept of periodicity is incorporated. The presented algorithm is illustrated in Section 4 by means of two industrially relevant examples based on the generation of microstructures for given particle size distributions of quartz sand and typical concrete aggregates. In Section 5 we discuss the future potential of the suggested rve generation scheme.



DOI: 10.1002/nag

## 2. GENERATION OF REPRESENTATIVE VOLUME ELEMENTS

Within the Lubachevsky–Stillinger algorithm, the generation of a representative volume element is accomplished by employing an event-driven scheme advancing from event to event, see Lubachevsky *et al.* [10–12]. Here, an event is considered to be the discrete collision between two particles. Each event is considered individually and in serial, postulating that only one discrete event is taking place at one discrete time. This leads to the possibility to handle each event individually. The basic steps of finding and handling an event are specified in Sections 2.1 and 2.2, whereas the algorithm used to produce the rve is described in Section 2.3.

### *2.1. Event-driven time step calculation*

In an event-driven scheme, the particles evolve independently at all time except for discrete asynchronous instances of pairwise interactions. The time step size is thus governed by the sequence of events. To calculate the time step $\Delta t$ which is needed to advance the particle system from time $t^n$ (Figure 1, left) to time $t^{n+1}$ (Figure 1, right) the event, collision between two particles, has to be observed. Since we are using a hard contact model we do not allow for particle overlap. Entering at time $t^n$ we assume that the positions of the particle centres $\mathbf{x}_i^n$, the particle radii $r_i^n$ as well as the particle velocities $\mathbf{v}_i^n$ are known. The key idea of the present rve generation scheme is that the initial individual particle radii are set to zero such that *ab initio* the particles are not in contact. The particle radii $r_i$ are then assumed to increase as

$$\dot{r}_i = g_i \quad \forall\, i \in \{1, \ldots, \mathsf{nop}\}, \quad r_i,\, g_i \in \mathbb{R} \tag{1}$$

The volume fraction $\phi$, i.e. the volume occupied by the particles per volume of the periodic boundary box is thus controlled by the growth rate $g_i$. If $g_i$ is equal for all particles $i$, a monodisperse packing is constructed, while different growth rates $g_i$ generate a multi-disperse packing, see Kansal *et al.* [20]. The discrete counterpart of (1) can be constructed, e.g. with the help of a finite difference scheme, i.e. $\dot{r}_i \approx [r_i^{n+1} - r_i^n]/\Delta t$, yielding the discrete update equation

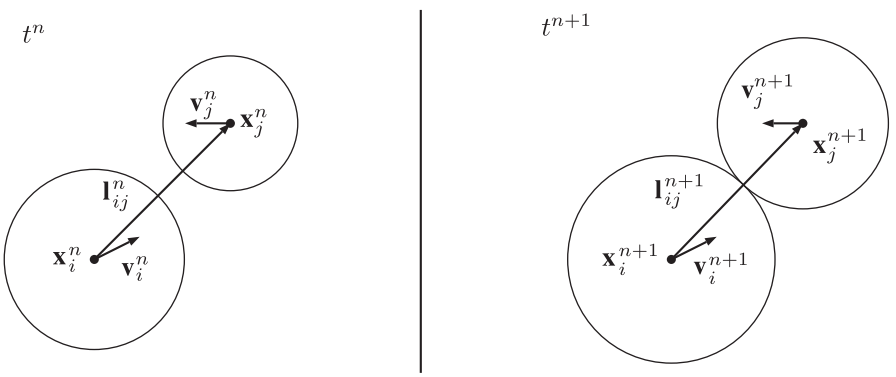


Figure 1. Configuration of particle $i$ and $j$ at time $t^n$ prior to contact and at $t^{n+1}$ defining the time step size $\Delta t$ due to the event 'particles in contact'.



DOI: 10.1002/nag

of the particle radii at time $t^{n+1}$:

$$r_i^{n+1} = r_i^n + g_i \, \Delta t \quad \forall \, i \in \{1, \ldots, \mathsf{nop}\} \tag{2}$$

Postulating a constant velocity of particle $i$ between the time nodes, the position of particle $i$ at time $t^{n+1}$ is calculated by using the well-known forward Euler formula:

$$\mathbf{x}_i^{n+1} = \mathbf{x}_i^n + \Delta t \; \mathbf{v}_i^n \quad \forall \, i \in \{1, \ldots, \mathsf{nop}\}, \quad \mathbf{x}_i, \mathbf{v}_i \in \mathbb{R}^{\mathsf{dim}} \tag{3}$$

The branch vector $\mathbf{l}_{ij}^{n+1}$ which connects the centres of the particles $i$ and $j$ is calculated by subtracting the position vectors of the particles:

$$\mathbf{l}_{ij}^{n+1} = \mathbf{x}_j^{n+1} - \mathbf{x}_i^{n+1} \quad \forall \, i \neq j, \quad i, j \in \{1, \ldots, \mathsf{nop}\} \tag{4}$$

For the sum of the particle radii being equal to the length of the branch vector, $\| \mathbf{l}_{ij}^{n+1} \| = r_i^{n+1} + r_j^{n+1}$, particles $i$ and $j$ are in contact, see Figure 1, right. Using (2) and (3) we can define the relevant time step size for the event-driven scheme $\Delta t$

$$\Delta t = \min_{\Delta t > 0} \left\{ \frac{[-\mathsf{v} \pm \sqrt{\mathsf{v}^2 - \mathsf{uw}}]}{\mathsf{u}} \right\} \tag{5}$$

with

$$\mathsf{v} = \mathbf{l}_{ij}^n \cdot [\mathbf{v}_j^n - \mathbf{v}_i^n] - [r_i^n + r_j^n][g_i + g_j] \tag{6}$$

$$\mathsf{u} = [\mathbf{v}_j^n - \mathbf{v}_i^n]^2 - [g_i + g_j]^2 \tag{7}$$

$$\mathsf{w} = \mathbf{l}_{ij}^{n\,2} - [r_i^n + r_j^n]^2 \tag{8}$$

The minimum of the two possible solutions for all possible particle contacts of the system defines the first contact and thus the time needed to advance to the next event.

### 2.2. *Event handling*

Being able to advance to the next event, the event itself has to be handled. Contact will be treated as a purely elastic impact between two bodies of equal mass. By taking into account the additional increase in size of the two colliding particles, the relation between the particle normal velocities directly before and right after the collision can be formulated as

$$\overset{+}{v}{}_{\mathrm{n}_i}^{n+1} = \mathsf{min} \left\{ \overset{-}{v}{}_{\mathrm{n}_i}^{n+1}, \overset{-}{v}{}_{\mathrm{n}_j}^{n+1} \right\} - g_i, \quad \overset{+}{v}{}_{\mathrm{n}_j}^{n+1} = \mathsf{max} \left\{ \overset{-}{v}{}_{\mathrm{n}_i}^{n+1}, \overset{-}{v}{}_{\mathrm{n}_j}^{n+1} \right\} + g_j \tag{9}$$

in terms of the growth rate $g_i$ and the normal contact velocity

$$v_{\mathrm{n}}^{n+1} = \mathbf{v}^{n+1} \cdot \mathbf{n}_{ij}^{n+1} \quad \text{with } \mathbf{n}_{ij}^{n+1} = \mathbf{l}_{ij}^{n+1} / \| \mathbf{l}_{ij}^{n+1} \| \tag{10}$$



DOI: 10.1002/nag

INITIALIZATION
random positions $\mathbf{x}_i^0$ , random velocities $\mathbf{v}_i^0$ , radii $r_i^0 = 0$, growth rates $g_i \in \mathsf{R}$

REPEAT
- select minimum collision time of all possible collisions (5)
- advance all particle positions regarding the minimum collision time (3)
- update velocity of colliding particle pair (9)

UNTIL $\Delta\phi < \Delta\phi^{\mathsf{crit}}$

Figure 2. Basic algorithm to produce dense particle packings by using a periodic boundary box. The dropout criterion, regarding the REPEAT UNTIL loop, is based on the increase of the volume fraction $\Delta\phi$, see (11).

Herein, $\overset{-}{(\bullet)}$ indicates quantities prior and $\overset{+}{(\bullet)}$ posterior to the collision. The assumption of the smoothness of the particles leaves the tangential particle velocities unchanged.

### 2.3. Event-driven generation of the rve

For simplicity, the rve is set to be a square with dimensions $\mathsf{l}_{\mathsf{rve}} \times \mathsf{l}_{\mathsf{rve}}$; however, any reasonable shape is possible. The desired number of particles is randomly distributed inside the periodic boundary box, initialized with random particle velocities. Radii of all particles are set to zero. Of interest is the next particle pair collision and its time. The time step calculation outlined in Section 2.1 is performed for each particle pair being able to collide. Different algorithms for fast collision detection can be found in the literature [21]. We use a parallelized screening contact detection algorithm, the search time is of the order $\mathcal{O}(\mathsf{nop})$. The minimum time step of all possible collisions, calculated by (5), is selected to advance the event-driven scheme. Next, all particle positions $\mathbf{x}_i^{n+1}$ are updated in terms of a forward Euler scheme (3). The post contact velocities of the colliding particle pair are determined according to (9), followed by a new search for the next collision. Allowing the algorithm to take its course, the particles float around inside the rve, collide and grow depending on the elapsed time. Postulation of a dropout criterion can be accomplished in many ways. We select the increase of volume fraction

$$\Delta\phi = \phi^{n+1} - \phi^{n+1-c} \quad \text{with} \quad \phi^{n+1} = \frac{\mathsf{v}_{\mathsf{par}}^{n+1}}{\mathsf{v}_{\mathsf{rve}}} = \frac{\pi}{\mathsf{v}_{\mathsf{rve}}} \sum_{i=1}^{\mathsf{nop}} r_i^{n+1\,2} \tag{11}$$

to be the variable of interest. With $\Delta\phi$ dropping under a certain threshold over a specified number of events, $c$ fulfils our criterion. The complete algorithm is listed in Figure 2.

## 3. CONCEPT OF PERIODICITY

In contrast to most existing rve generation strategies in the literature, our algorithm essentially generates periodic microstructures which can eventually be used for multiscale simulations on the



DOI: 10.1002/nag

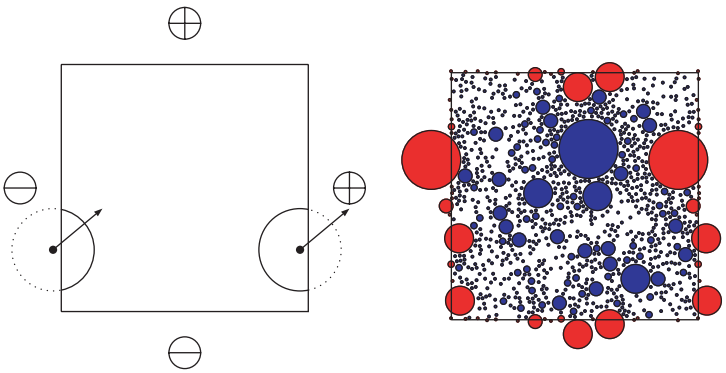

Figure 3. Left: schematic illustration of a periodic boundary box including one primary particle and its replica. Right: computational realization including 1000 primary and 34 replica particles with volume fraction $\phi \approx 0.45$.

integration point level of large-scale finite element simulations, see e.g. Dettmar and Miehe [18] for typical examples. We thus aim at generating a geometrically periodic rve. Its construction typically starts with the definition of a periodic boundary box, see Figure 3. Topologically speaking, the periodic boundary box for two-dimensional systems can be thought of as a torus with particles moving on the torus surface. The torus is set up by connecting the opposite boundary box sides marked by $\ominus$ and $\oplus$. A particle with its centre being inside the boundary box is considered to be a primary particle. If a primary particle intersects with a boundary of the periodic boundary box, a replica of this particle is positioned on the opposite side. All properties of the primary particle are projected onto the replicated particle. As soon as the centre of the primary particle leaves the boundary box, the replicated particle centre enters the boundary box and their states change. This leads to a constant number of primary particles inside the periodic boundary box. The periodic boundary box is used as a frame for the periodic rve.

## 4. EXAMPLES

Finally, the features of the suggested Lubachevsky–Stillinger algorithm will be illustrated by means of two selected representative examples, one from soil mechanics, the other one from the materials science of concrete. A common means to classify particular granular media is their grain size distribution in the form of sieve curves. Typical sieve curves are depicted in Figure 4. The diagram on the left shows a characteristic grain size distribution of a quartz sand, whereas, the diagram on the right depicts a concrete aggregate distribution required to ensure concrete of a particular quality. These curves which can be taken from German DIN standards [22] depict the volume percentage of particles passing sieves of particular diameters plotted over the individual sieve diameters. As such, they have to be converted to provide the appropriate input format for our particular rve generation algorithm. To begin with the volume percentage of passing particles needs to be extracted for each grain size fractions of Figure 4. With the individual volume percentages passing per grain size fraction at hand the particle percentage per grain size fraction can be calculated



DOI: 10.1002/nag

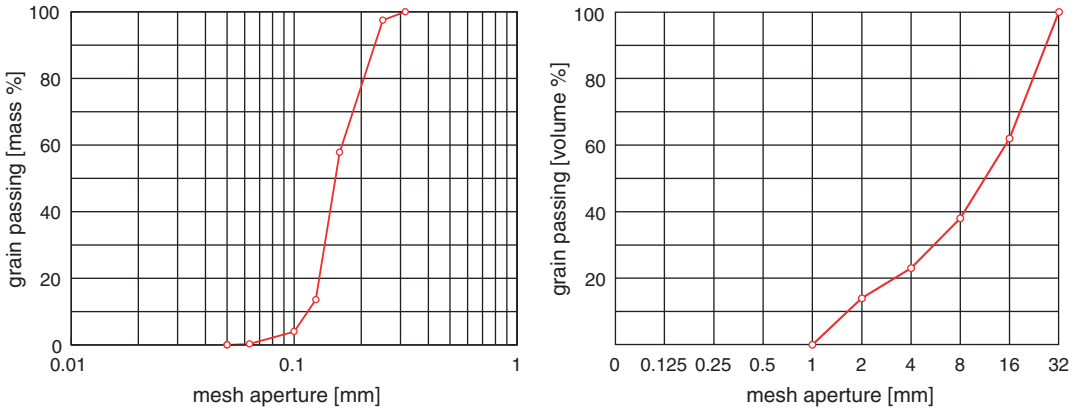


Figure 4. Grain size distributions. Left: quartz sand, grain passing in mass percent over mesh aperture. Right: A32 from German standard DIN 1045. The abscissa shows the mesh aperture in (mm), whereas the ordinate reads the grain passing in volume percent.

as follows:

$$\text{particle } \%_i(\varnothing_i) = \frac{\dfrac{\text{volume } \%_i}{\varnothing_i^2}}{\displaystyle\sum_j \frac{\text{volume } \%_j}{\varnothing_j^2}} \tag{12}$$

To select the minimal number of particles needed to include at least one particle of each grain size fraction, the following equation

$$\text{nop}_{\min} = \left[ \min_{\text{particle } \%_i > 0} \{\text{particle } \%_i(\varnothing_i)\} \right]^{-1} \cdot 100 \tag{13}$$

needs to be evaluated. For a number of particles larger than $\text{nop}_{\min}$, the number of particles per grain size fraction follows straightforwardly by scaling the particle percentage derived by (12). The growth rate $g_i$ of each particle $i$ is set to be equivalent to the expected particle diameter itself. This approach guarantees the preservation of a scaled version of the prescribed grain size distribution during the evolution process. Note the importance of keeping the ratios between the growth rates equal to the ratios between the different grain sizes. In what follows, we elaborate the rve generation based on the two given sieve curves given in Figure 4. Please note that the simulation states with low densities, depicted in Figures 5 and 7, are only algorithmic intermediate configurations. The interest of our simulation is focused on the final state.

### *4.1. Grain size distribution of quartz sand*

The first example is taken from the field of geomechanics. In this case we selected a grain size distribution of a quartz sand provided by the Institute of Foundation Engineering and Soil Mechanics of the Ruhr-University Bochum, see Wichtmann [23]. The chosen quartz sand is distinguished by a low non-uniformity index of 1.4 and a mean diameter of 0.15 mm. The related sieve curve is illustrated in Figure 4, left. Its evaluation renders the relevant grain diameters and



DOI: 10.1002/nag

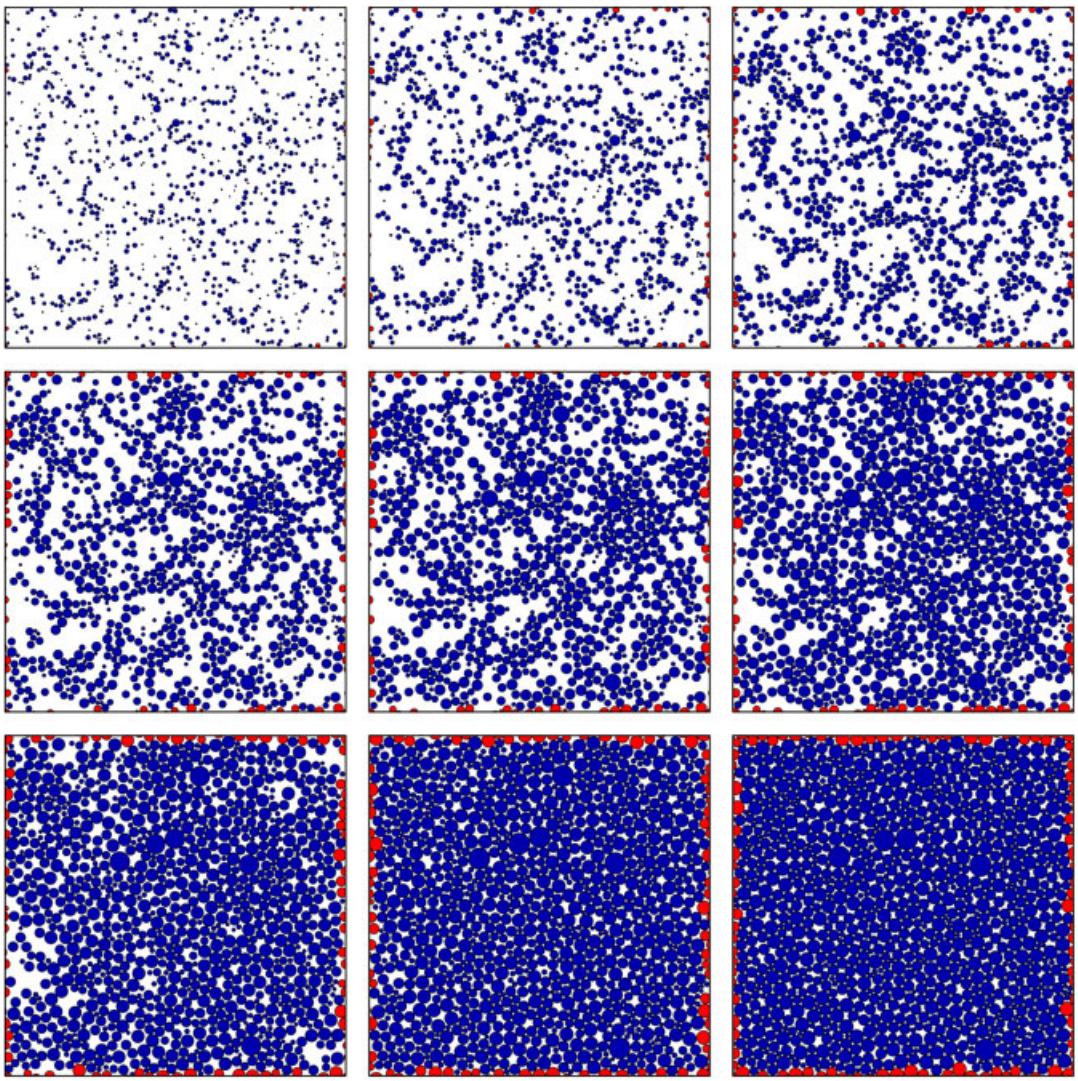

Figure 5. Evolution process of a multi-disperse rve containing 1000 primary particles, started with values of Table I. Particles inside the rve are coloured in blue (dark grey), particles intersecting with the periodic boundary box are coloured in red (light grey). The periodic boundary box is illustrated by a black frame. The evolution is depicted from the upper left to the lower right image. The corresponding volume fractions start with $\phi = 0.1$, advance with $\Delta\phi = 0.1$ and reach a final $\phi \approx 0.847014$ in the lower right image.

the corresponding mass and volume percentage as columns I, II and III of Table I. The particle percentage summarized in column IV follows straightforwardly from Equation (12). Its scaling renders the number of particles per grain fraction for a total number of particles of $\mathsf{nop} = 1000$, see column V. A series of different stages of the rve generation process based on the initialization of Table I is shown in Figure 5. The series starts in the upper left corner with an overall volume



DOI: 10.1002/nag

Table I. One thousand primary particles, quartz sand example.

| Grain ∅ (mm) | Mass % (%) | Volume % (%) | Particle % (%) | Particle (dimensionless) |
|---|---|---|---|---|
| 0.315 | 0.00 | 0.00 | 0.0000 | 0 |
| 0.250 | 2.50 | 2.50 | 0.6227 | 6 |
| 0.160 | 39.72 | 39.72 | 24.1531 | 242 |
| 0.125 | 44.22 | 44.22 | 44.0557 | 441 |
| 0.100 | 9.58 | 9.58 | 14.9131 | 149 |
| 0.063 | 3.70 | 3.70 | 14.5119 | 145 |
| 0.050 | 0.28 | 0.28 | 1.7435 | 17 |

fraction of $\phi = 0.1$ increasing up to $\phi = 0.8$ by $\Delta\phi = 0.1$ from one snapshot to the next. The final distribution in the lower right corner which can be interpreted as a closest packing for the given sieve curve corresponds to a volume fraction of $\phi = 0.847014$. In the early stages of the evolution process, particles move freely from collision to collision. Fluid- or gas-like behaviour is noticed, keeping in mind the unphysical gain of energy. At these stages, no oscillations of the particles are noticed. As the particle radii increase, the space available for particles to move becomes limited. This point is distinguished by a high oscillation of particles resulting in a drastically decreasing time step sizes $\Delta t$. The drastic changes in the time step size indicate the region of liquid–solid transformation, studied in [24]. These stages roughly corresponds to the lower row of snap shots in Figure 5 related to overall volume fractions of $\phi > 0.7$. From this point on, the rve generation process is dominated by shifts of patterns and reorganization of larger subunits. Due to the close packing of particles, time between collisions narrows down quickly. Accordingly, the individual particles hardly increase in size anymore and the overall volume fraction tends to saturate. The largest packing density of $\phi = 0.847014$ is defined algorithmically in terms of the incremental increase in volume fraction dropping below the critical value of $\Delta\phi^{\text{crit}} = 1.0\text{E} - 09$.

The evolution of the time step size $\Delta t$ is depicted in Figure 6. For each subsequent event, the time step size is indicated by one single dot in the diagram. The abscissa thus illustrates the number of relevant events starting from one increasing up to almost $1.6\text{E} + 07$ from left to right. It is obvious that the time step size decreases drastically during the onset of the rve generation procedure. After approximately $1.6\text{E} + 07$ events, the time step size has converged towards an almost constant value somewhat below $1.0\text{E} - 10$. Figure 6 nicely demonstrates why our definition of algorithmic convergence in terms of the critical value $\Delta\phi^{\text{crit}}$ as introduced in Equation (11) is indeed a reasonable choice. Generally, one could be tempted to use the readily available time step size as a criterion for convergence. However, the diagram in Figure 6 shows that due to the stochastic nature of the contact distribution, the choice of a single absolute convergence criterion might have stopped the simulation long before overall convergence is observed. Accordingly, controlling an integral value which has been replaced by its discrete counterpart in form of a sum in Equation (11) seems a suitable choice.

### *4.2. Grain size distribution of concrete aggregates*

The second example of concrete aggregates is more spectacular since its the overall particle size distribution is much more non-uniform than in the previous example. Figure 4, right, represents a concrete aggregate distribution curve taken from the German standard DIN 1045. Here we selected



DOI: 10.1002/nag

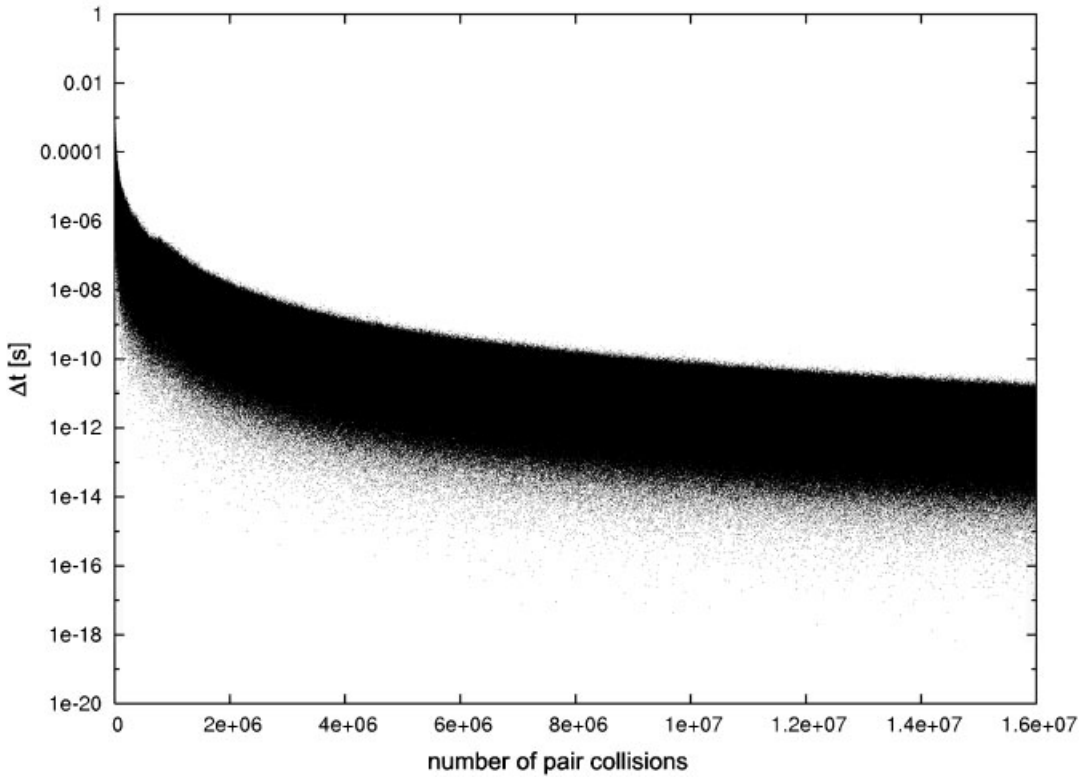


Figure 6. Time step size over number of particle pair collisions, quartz sand. Each time step size $\Delta t$ is represented by one single dot.

Table II. One thousand primary particles, concrete example.

| Grain ∅ (mm) | Volume % (%) | Particle % (%) | Particle (dimensionless) |
|---|---|---|---|
| 32 | 0 | 0.0000 | 0 |
| 16 | 38 | 0.8381 | 8 |
| 8 | 24 | 2.1173 | 21 |
| 4 | 15 | 5.2933 | 53 |
| 2 | 9 | 12.7040 | 127 |
| 1 | 14 | 79.0472 | 791 |

the coarse-grained sieve curve A32, with the largest grain having a diameter of 32 mm. For practical reasons, we restricted the finest grain to have a diameter of 1 mm. Columns I and II of Table II summarize the grain diameters and their corresponding volume percentage. The particle percentage of column III can be calculated with the help of Equation (12). Again, we assume a representative number of particles of $\mathsf{nop} = 1000$ and obtain the absolute number of particles for each grain size which is one-to-one related to the individual growth rates $g_i$, compare column IV.



DOI: 10.1002/nag

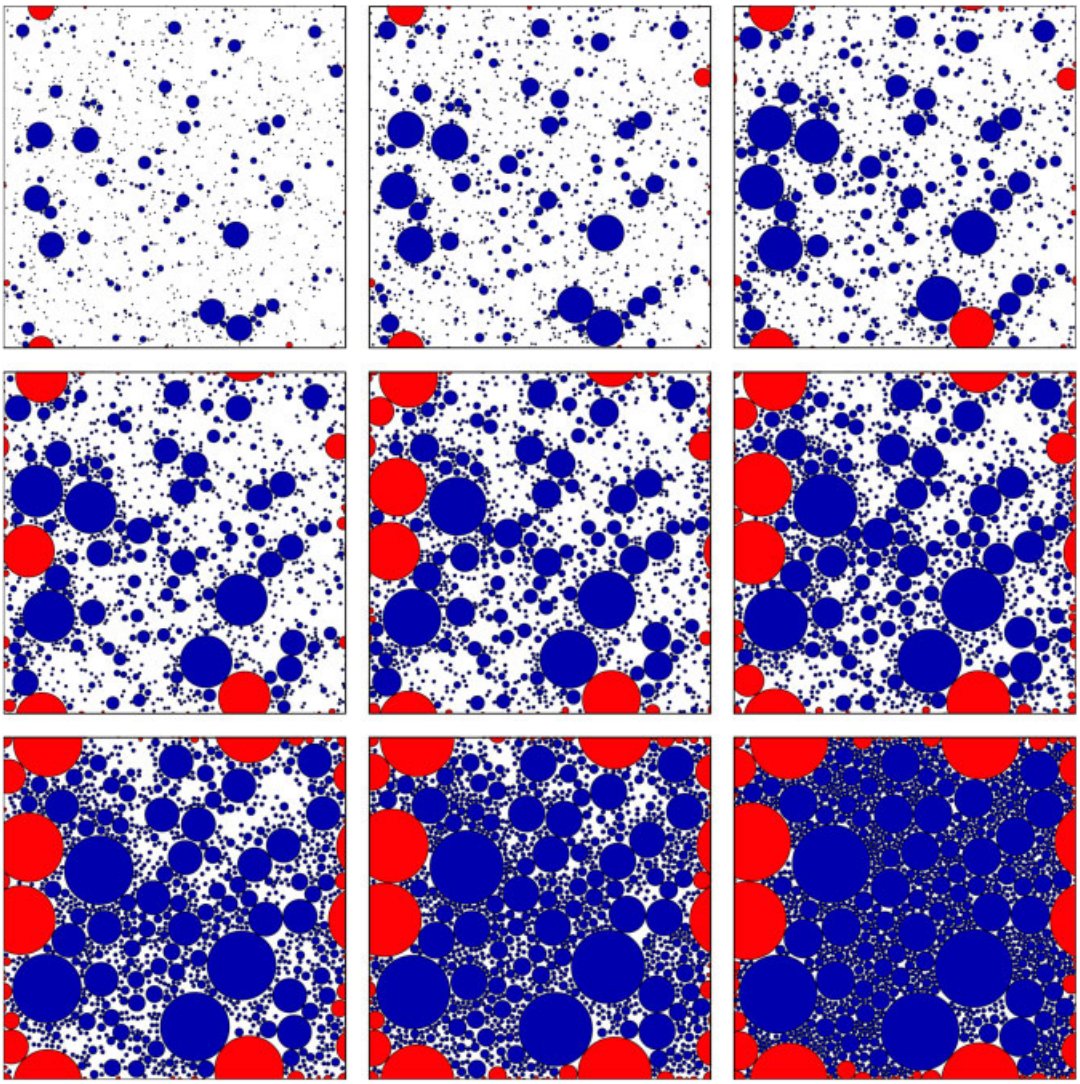

Figure 7. Evolution process of a multi-disperse rve containing 1000 primary particles, launched with values of Table II. Particles inside the rve are coloured in blue (dark grey), particles intersecting with the quadratic periodic boundary box are coloured in red (light grey). The periodic boundary box is illustrated by a black frame and has dimensions 100. The evolution is depicted from the upper left to the lower right image. The corresponding volume fractions start with $\phi = 0.1$, advance with $\Delta\phi = 0.1$ and reach $\phi = 0.9$ in the lower right image. All images are cropped at the outline of the quadratic periodic boundary box. The final rve is shown in Figure 8, right.

Figure 7 illustrates the generation procedure for the concrete aggregate rve. The upper left corner corresponds to a volume fraction of $\phi = 0.1$ which increases by $\Delta\phi = 0.1$ from one image to the next. The final snap shot thus corresponds to an overall volume fraction of $\phi = 0.9$. The largest



DOI: 10.1002/nag

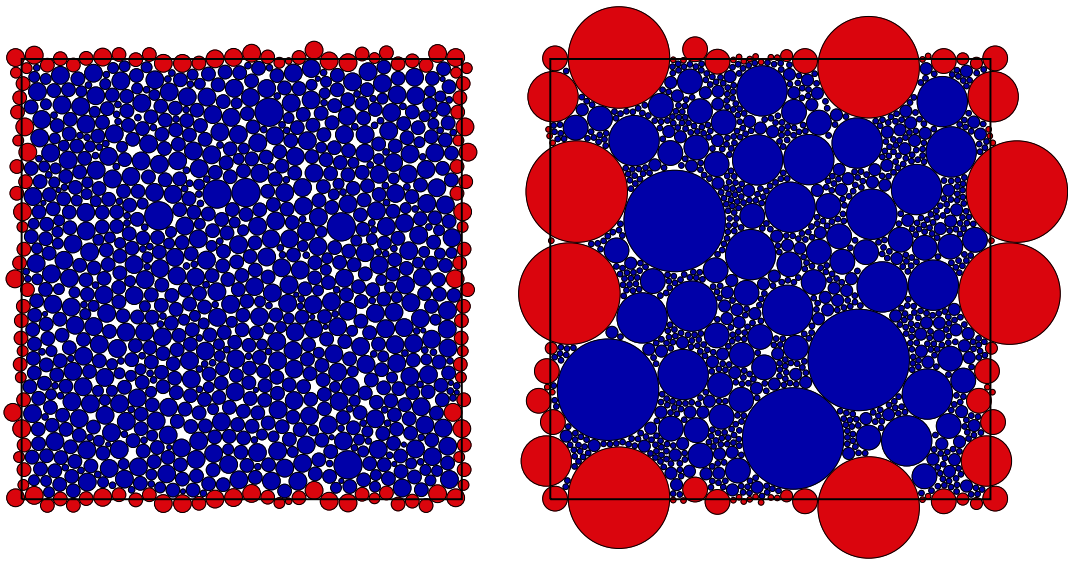

Figure 8. Final rves including 1000 primary particles. Left: quartz sand; right: concrete aggregate.

packing density found algorithmically on the basis of the convergence criterion $\Delta\phi^{\text{crit}} = 1.0\text{E}-09$ was found to be slightly larger at $\phi \approx 0.914793$, see Figure 8. In contrast to the previous example of a rather uniform quartz sand, the aggregate size distribution in concrete is extremely heterogeneous. It is quite obvious that this heterogeneity allows for larger packing densities which is, of course, a desired property for high-performance concrete. The question of how much disorder is needed to avoid ordering effects is discussed in [24]; in this short communication we simply handle given grain size distributions to produce heterogeneous packings. Algorithmically, heterogeneous multi-dispersechallenging than almost uniform or even entirely monodisperse packings. Particle collisions are more likely to take place at the early stages of the generation process. Accordingly, in general, smaller time steps are needed, even at the early low-density stages. Another distinguishing feature of heterogeneous multi-disperse is their ability to pack very densely. Accordingly, clustering and formation of subunits are less likely as compared to uniform or even monodisperse packings. It is quite obvious that the time step size related to the final snap shot of Figure 7 at a packing density of $\phi = 0.9$ is extremely small. Nevertheless, we should keep in mind that realistic aggregate volume fractions in concrete typically lie within the range of $0.65 \leqslant \phi \leqslant 0.85$ corresponding to the first and second snap shot in the lower row of Figure 7. The final stages of the generation process that are represented by the final snap shot are extremely expensive from a computational point of view but fortunately they are rather of academic nature.

A distinguishing quality feature of rve generation algorithms is their ability to densely populate the boundary box of the rve. Typically, the ultimate goal of the rve generation process is to subject the generated substructure to selected mechanical loading scenarios such as simple shear, pure shear, compression or combinations thereof. The quality of the final rve thus strongly depends on a full boundary set $\mathscr{B} := \{i \in \{1, \ldots, \text{nop}\} : \overline{B}_{R_i}(\mathbf{x}_i^0) \cap \partial\text{rve} \neq \emptyset\}$. Set $\mathscr{B}$ is considered a full set algorithmically, if the gap between each particles of set $\mathscr{B}$ is less than the sum of the two neighbouring particle radii plus the smallest particle diameter within the entire rve. The condition



DOI: 10.1002/nag

of a full set $\mathscr{B}$ ensures that no particles inside can escape the boundary box when subjected to shear or compression. Various different studies showed that our algorithm generally satisfies this essential feature of generating full sets. Figure 8 depicts the full boundary sets of the final rves of the quartz sand example, left, and of the concrete aggregate example, right. In the case of a non-full boundary set $\mathscr{B}$, additional care would have to be spent on ensuring that the possible outgoing mass flux is equivalent to its incoming counterpart.

## 5. CONCLUSION

The generation of geometrically periodic random representative volume elements is of general interest for various different applications of granular media. Motivated by the Lubachevsky–Stillinger algorithm developed in the context of computational chemistry we discuss a strategy to generate periodic microstructures with the ultimate goal of incorporating them as representative volume elements on the integration point level in an overall finite element analysis at later stages of this research. The representative volume elements generated by the Lubachevsky–Stillinger algorithm show a number of distinguishing features that seem highly attractive in particular for applications in geomechanical areas: they are geometrically periodic, heterogeneous, densely packed full sets which essentially reflect user-defined grain size distribution patterns. Technically speaking, the underlying algorithm is embedded in a serial event-driven scheme starting with a random spatial distribution of particles of size zero. The particle size increases systematically as time evolves whereby each particle has to be assigned a characteristic growth rate. These individual particle growth rates can be extracted through a one-to-one mapping from prescribed grain size distributions which essentially govern the random heterogeneity of the microstructure. Accordingly, basically any given sieve curve can be accounted for naturally and the generation of monodisperse as well as multi-disperse packings of various degrees of heterogeneity is straightforward. Unless the final packing density is prescribed externally, for example, when generating a particular concrete microstructure with a given aggregate volume fraction, the algorithm was shown to produce remarkably large packing densities. For an overall particle volume fraction larger than 0.8, not only the interior of the rve but also its boundary are extremely densely populated. This feature is essentially important when keeping in mind the overall goal of this study in which the generated rve is to be subjected to selected mechanical loading scenarios: a densely populated boundary, or rather a full set, ensures that small particles cannot leave the sample in response to external compression or shear loading. Due to the underlying algorithmic simplicity, the present algorithm is believed to be a first step to provide a stable and efficient tool to generate random geometrically periodic microstructures that will be extremely useful in different areas of computational physics, geomechanics, concrete design, material modelling and homogenization.

ACKNOWLEDGEMENTS

The authors thank the German Research Foundation (DFG) for financial support within the DFG International Research Training Group 1131, 'Visualization of Large and Unstructured Data Sets Applications in Geospatial Planning, Modeling and Engineering' at the University of Kaiserslautern. Furthermore, we would like to acknowledge Prof. T. I. Zohdi of the University of California, Berkeley, for his outstanding cooperation.



DOI: 10.1002/nag

## REFERENCES


1. Cundall PA, Strack ODL. The distinct element method as a tool for research in granular media. *Report to the National Science Foundation Concerning NSF Grant ENG76-20711*, *PART I*, 1978.
2. Cundall PA, Strack ODL. The distinct element method as a tool for research in granular media. *Report to the National Science Foundation Concerning NSF Grant ENG76-20711*, *PART II*, 1979.
3. Zohdi TI, Wriggers P. *Introduction to Computational Micromechanics*. Springer: Berlin, 2005.
4. Zohdi TI. Modeling and direct simulation of near-field granular flows. *International Journal of Solids and Structures* 2005; **42**:539–564.
5. Zohdi TI. Charge-induced clustering in multifield particulate flow. *International Journal for Numerical Methods in Engineering* 2005; **62**:870–898.
6. Luding S. From microscopic simulations to macroscopic material behavior. *Computer Physics Communications* 2002; **147**:134–140.
7. Luding S. Micro–macro transition for anisotropic, frictional granular packings. *International Journal of Solids and Structures* 2004; **41**:5821–5836.
8. Stroeven M, Askes H, Sluys LJ. Numerical determination of representative volumes for granular materials. *Computational Methods for Applied Mechanics and Engineering* 2004; **193**:3221–3238.
9. Gitman IM, Gitman MB, Askes H. Quantification of stochastically stable representative volumes for random heterogeneous materials. *Archive of Applied Mechanics* 2006; **75**:79–92.
10. Lubachevsky BD, Stillinger FH. Geometric properties of random disk packings. *Journal of Statistical Physics* 1990; **60**:561–583.
11. Lubachevsky BD. How to simulate billiards and similar systems? *Journal of Computational Physics* 1991; **94**:255–283.
12. Lubachevsky BD, Stillinger FH, Pinson EN. Disks vs spheres: contrasting properties of random packings. *Journal of Statistical Physics* 1991; **64**:501–524.
13. Meier HA, Kuhl E, Steinmann P. Failure of granular materials at different scales—microscale approach. *PAMM* 2006; **6**:399–400.
14. Meier HA, Kuhl E, Steinmann P. On discrete modeling and visualization of granular media. In *Visualization of Large and Unstructured Data Sets, GI-Edition*, Hagen H, Kerren A, Dannenmann P (eds). Lecture Notes in Informatics, Gesellschaft für Informatik: Bonn, 2006; 165–175.
15. Brunner M, Bechinger C, Herz U, Grunberg HH. *Europhysics Letters* 2003; **63**(6):791–797.
16. Lätzel M, Luding S, Herrmann HJ. From discontinuous models towards a continuum description. *Lecture Notes in Physics*, vol. 568. Springer: Berlin, 2001; 215–230.
17. Luding S, Santos A. Molecular dynamics and theory for the contact values of the radial distribution functions of hard-disk fluid mixtures. *Chemical Physics* 2004; **121**(17):8458–8465.
18. Dettmar J, Miehe C. A framework for micro–macro transitions in periodic particle aggregates of granular materials. *Computer Methods in Applied Mechanics and Engineering* 2004; **193**:225–256.
19. Baram RM. Polydisperse granular packings and bearings. *Dissertation*, Institute für Computeranwendungen 1, Universität Stuttgart, 2005.
20. Kansal AR, Torquato S, Stillinger FH. Computer generation of dense polydisperse sphere packings. *Journal of Chemical Physics* 2002; **117**(18):8212–8218.
21. Munjiza A. *The Combined Finite-Discrete Element Method*. Wiley: New York, 2004.
22. DIN Deutsches Institut für Normung e.V. DIN 1045-2 Tragwerke aus Beton, Stahlbeton und Spannbeton, Teil 2: Beton—Festlegung, Eigenschaften, Herstellung und Konformität, Anwendungsregeln zu DIN EN 206-1 Beuth Verlag GmbH, Berlin, 2001.
23. Wichtmann T. *Explicit Accumulation Model for Non-cohesive Soils under Cyclic Loading*. Schriftreihe des Institutes für Grundbau und Bodenmechanik der Ruhr-Universität Bochum, Heft 38, 2005.
24. Luding S. Liquid–solid transformation in bidisperse granulates. *Advances in Complex Systems* 2002; **4**:379–388.




DOI: 10.1002/nag